

## Nonuniformities in the Angle of Repose and Packing Fraction of Large Heaps of Particles

Nikola Topić,<sup>1</sup> Jason A. C. Gallas,<sup>1,2</sup> and Thorsten Pöschel<sup>1,2</sup>

<sup>1</sup>*Institute for Multiscale Simulations, Friedrich-Alexander-Universität, D-91052 Erlangen, Germany*

<sup>2</sup>*Departamento de Física, Universidade Federal da Paraíba, 58051-970 João Pessoa, Brazil*

(Received 22 December 2011; published 19 September 2012)

We report a numerical investigation of the structural properties of very large three-dimensional heaps of particles produced by ballistic deposition from extended circular dropping areas. Very large heaps are found to contain three new geometrical characteristics not observed before: they may have two external angles of repose, an internal angle of repose, and four distinct packing fraction (density) regions. Such characteristics are shown to be directly correlated with the size of the dropping zone. In addition, we also describe how noise during the deposition affects the final heap structure.

DOI: [10.1103/PhysRevLett.109.128001](https://doi.org/10.1103/PhysRevLett.109.128001)

PACS numbers: 45.70.Cc, 45.70.Vn, 61.43.Bn

Heaps of granular particles have been studied intensively during the past few decades both because of their great relevance for industrial applications and because, from a theoretical point of view, heaps are simple many-body systems well suited to develop and probe theories [1,2]. The formation of grain heaps is of paramount importance to understand theoretically and experimentally complex cooperative phenomena. Examples of complex granular phenomena that attracted recurring interest over the years include the perennial quest for the characterization of the stress dip under the pile [3–8], avalanching behavior [9,10], segregation by size [11–13], creep motion deep in the pile [14] and the remarkable properties discovered in the growth of grain piles by revolving rivers [15–18], and several others [19,20].

Most of the results obtained so far are for two-dimensional (2D) heaps of grains. For instance, very recently Roul *et al.* [21] studied packing properties of 2D piles of grains using sophisticated molecular dynamic simulations. Among other things, they reported the presence of a clear peak in the particle density around the middle of the heap arguing that local compactification and arching could perhaps explain such differences. Variations in the angle of repose of 2D heaps were investigated as a function of experimental parameters and deviations in the shape of the tail of 2D sandpiles were discovered [22]. Experiments and theory concerning the pressure dip under 2D grain piles along with some results for three-dimensional (3D) heaps were reported by Atman *et al.* [4] who found the controversial presence or absence of pressure dips to be closely related to the preparation history of the pile and called for more extensive systematic studies.

A major factor determining the pile structure is the force that it experiences during the deposition process. Lateral forces constraining 2D piles are quite different from lateral forces in 3D piles. So, it seems natural to investigate systematically the structure of 3D packings subjected to more complex lateral forces and to see whether they imply

hitherto unnoticed features. Although static piles of granular materials are classical examples of packings, to date there has been no systematic study of spatially resolved packing properties of 3D heaps. Three-dimensional packings require using a large number of particles, of the order of two to three orders of magnitude more than in 2D scenarios.

Here we report a study of the density distribution and the angle of repose measured for very large 3D heaps of monodisperse spherical particles, as illustrated in Fig. 1. We report results obtained for heaps with up to  $25 \times 10^6$  particles dropped sequentially onto a horizontal plane from a homogeneous “rain” of particles emerging from a circular area source with adjustable radius. Of main interest is to determine bulk properties such as density, contact numbers, repose angles, etc. Three-dimensional simulations are hardly feasible with a full molecular dynamics approach, but there are efficient alternative ways to address the problem. However, simpler models for ballistic deposition and related surface growth problems can provide useful insight for specific problems as the ones studied by us. Here we use the well-known Visscher-Bolsterli (VB) algorithm [10,13,23,24]. This algorithm was used in pioneering work by Jullien and Meakin [13] to study size segregation in 3D heaps with  $(4\text{--}40) \times 10^3$  particles. As mentioned, here we consider very large 3D heaps involving typically  $(10\text{--}25) \times 10^6$  particles. In the VB algorithm, the particles are dropped one by one onto a growing deposit (see Fig. 1). Particles follow the path of steepest descent until they stop after reaching either a local stable minimum or when touching the ground. After stopping, particles are not allowed to move anymore so that many-particle effects like, e.g., avalanches, cannot be simulated, although a plethora of other effects are nicely reproduced [10,13,24]. The key advantage of the sequential VB algorithm is that it provides a realistic framework to rapidly compute the path of steepest descent and, therefore, allows us to investigate very large assemblies of particles not accessible with other models. We now describe our main findings.

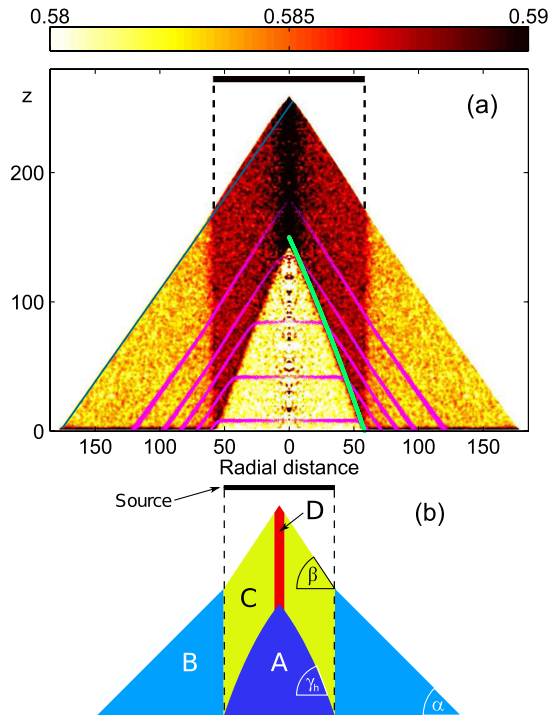


FIG. 1 (color online). (a) Packing fraction for a 3D heap with five contours superimposed showing the growth history and that the flat horizontal surface shrinks as the growth proceeds. The line segment on the right of the inner triangle shows the prediction of Eq. (1). Here  $N = 10^7$ . The auxiliary straight line on the left heap boundary helps the visualization of the two angles of repose. (b) Schematic representation of a generic heap and its main characteristics: the angles of repose  $\alpha$ ,  $\beta$ ,  $\gamma_h$ , where  $h$  is the height at which the angle is measured, and the four axially symmetric density zones A, B, C, D. The small curvature of the inner triangle A was enhanced for clarity. In all cases investigated it is well approximated by a straight line.

Figure 1(a) shows the packing fraction as a function of the radial distance from the heap axis for a 3D heap made of  $N = 10^7$  particles deposited sequentially from random positions in the extended circular source whose section is indicated by the solid black bar. To illustrate the growth history of the pile, we superimposed to it five contours showing the evolving shape obtained after depositing  $N = 10^5$ ,  $5 \times 10^5$ ,  $10^6$ ,  $1.6 \times 10^6$ , and  $3 \times 10^6$  particles. From these contours, one sees how the inner triangular density cone gets formed as the flat horizontal surface gets smaller and smaller when the particle deposition proceeds. The packing fraction was obtained using cylindrical coordinates  $(r, z, \phi)$  coaxial with the heap. For masses  $m_i$  with center of mass at  $\mathbf{r}_i$  we measured the density  $\rho(r, z, \phi)$  at  $\mathbf{r}$  using the definition [25]  $\rho(\mathbf{r}) \equiv \sum_i m_i \phi[\mathbf{r} - \mathbf{r}_i]$ , where  $\phi$  is a Gaussian coarse-graining function  $\phi = (1/\pi w^2) e^{-(|\mathbf{r}|/w)^2}$ ,  $w = 2R$ , and  $R$  is the particle radius. Then, by averaging  $\rho(r, z, \phi)$  over  $\phi$  we get the density distribution  $\bar{\rho}(r, z)$ , the quantity color coded in Fig. 1(a).

How does the packing fraction vary along large heaps produced by extended sources? This may be recognized both from the real heap in Fig. 1(a) and from the summarizing sketch in Fig. 1(b). In general, we find heaps to contain four distinct density (packing) regions: First, there is a triangular region A under the dropping zone. When A grows, particles may eventually move outside the “shadow” of the dropping source forming the packing zone B. Since in this zone the VB algorithm requires moving particles to always maintain contact with the heap, outside the shadow of the dropping zone there is a region B where the particles are arranged more regularly than in A, which grows on top of a randomly deposited initial layer. Next comes region C, an intermediary packing that is less regular than that of B but more regular than that of A. Finally, in D we find the highest density of the heap. For a heap with  $N = 10^7$  particles we find the following representative densities well inside each region:  $\rho_A = 0.5812 \pm 0.0002$ ,  $\rho_B = 0.5832 \pm 0.0002$ ,  $\rho_C = 0.5879 \pm 0.0002$ , and  $0.59 \pm 0.02 < \rho_D < 0.63 \pm 0.02$ . Approximating boundaries by straight lines, the corresponding angles of repose are  $\alpha = (54.5 \pm 0.5)^\circ$ ,  $\beta = (57.5 \pm 0.5)^\circ$ , and  $\gamma = (68 \pm 0.4)^\circ$ , measured directly from Fig. 1(a). The origin of the differences in density is the different mechanism of sedimentation. While sequential deposition means that particles following strictly the path of steepest descent, in the presence of noise, Fig. 3, means that occasionally the steepest descent is interrupted, placing the particle on a random position in a close neighborhood thereby allowing previously inaccessible minima to become accessible.

The distinct density zones described above have a remarkable implication for the angle of repose. Instead of the familiar single angle of repose, we find heaps in fact to display two external angles of repose along with an internal angle, the boundary between A and C in Fig. 1(b). As shown by the auxiliary line on the left side of the heap in Fig. 1(a), under the dropping zone one finds a larger angle than outside it. Noteworthy, there are two distinct limits of

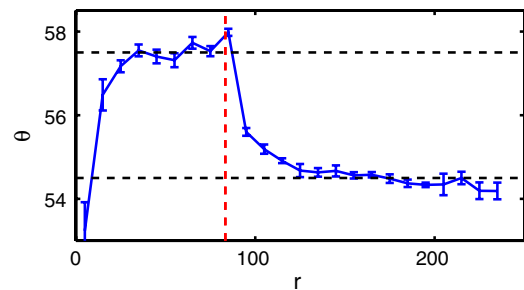


FIG. 2 (color online). Angle of repose  $\theta$  as a function of the distance  $r$  from the axis (in units of particle diameters) measured for a heap with  $N = 2.5 \times 10^7$  particles. The radius of the dropping zone is indicated by the vertical dashed line. Note the marked discontinuity between the angles indicate by the horizontal dashed lines.

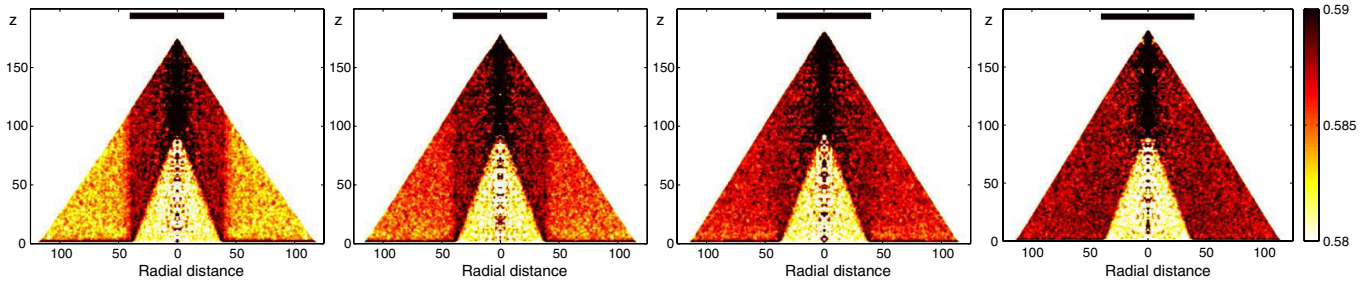


FIG. 3 (color online). Region  $B$  is overtaken by  $C$  as random noise during the deposition increases. In the leftmost panel the heap was never perturbed ( $e = \infty$ ). The other three panels, from left to right, show heaps formed when applying with an increasing frequency a random perturbation, namely, after every 512, 128, and 32 “events” (see text) corresponding, approximately, to particles traveling downwards for about 160, 40, and 10 particle diameters, respectively. Each panel displays  $N = 3 \times 10^6$  particles.

interest here. Region  $B$  overtakes  $C$  (and  $A$ ) when the drooping zone shrinks, or the contrary happens,  $C$  overtakes  $B$ , if the noise increases. The usual angle of repose is the final single angle obtained after taking anyone of these limits. We measured the pair of external angles as follows. For every  $z_i$ , we located the set of points  $r_i$  defining the outermost surface points around the heap, plotting them as  $r = r(z)$ . Then, using bins with  $\Delta r = 10$  particle diameters, we fitted a straight line through the points  $(r_i, z_i)$  for each bin obtaining the dependence of the local angle of repose  $\theta$  with distance from the axis.

Figure 2 shows the typical jumps observed in the angle of repose as a function of the radial distance in the heap. One clearly recognizes the difference of being inside and outside the rain of particles. Error bars represent the deviations recorded when sampling over five distinct heaps and show that the variations of the angles are much larger than the fluctuations resulting from sampling different heaps. The existence of two angles of repose can be observed qualitatively already in a “kitchen table” experiment (see Supplemental Material [26]).

Are angles of repose and density zones affected by random fluctuations during the deposition process due to, e.g., saltation of grains? To check this, we performed a numerical experiment which consisted of perturbing periodically the deposition process after the particle had a number  $e$  of “events” in the pile, i.e., after it had the opportunity of falling long enough so as to have changed its contacts  $e$  times on its way down. After falling down unperturbed for  $e$  events, the particle was then lifted vertically from its position  $(x, y)$  and dropped randomly at a nearby location  $(x + \Delta x, y + \Delta y)$ , where there are random numbers such that  $(\Delta x)^2 + (\Delta y)^2 < 9R^2$ , where  $R$  is the radius of the particles. Figure 3 illustrates the result of such experiment for increasing noise strength: one clearly sees that region  $B$  is overtaken by  $C$  as the perturbation frequency increases (from left to right). Since the correlation of the deposition process is destroyed by noise, Fig. 3 indicates that strong noise during the deposition is responsible for the increasingly higher density observed in the  $B$  zone (when compared with the density in  $C$ ). Remarkably,

zones  $A$  and  $D$  remain essentially unaffected by noise during the whole deposition process. Furthermore, one sees that deposition strongly affected by noise may prevent the observation of two angles of repose.

The average number of contacts among particles is a classic measure to characterize the packing structure of spheres [27]. Thus, we determined the average number of contacts in a similar way as described above for the density but, of course, replacing  $\rho(\mathbf{r})$  by  $c(\mathbf{r}) = (\sum_i c_i)/n$ , where  $c_i$  and  $\mathbf{r}_i$  are the number of contacts and position of particle  $i$ , and  $n$  is the total number of particles inside of the averaging volume. The result of such counting is given in Fig. 4 and is clearly consistent with our findings described above, in particular the geometrical picture summarized in Fig. 1(b).

In addition to the four areas in the packing fraction, the distribution of contact numbers in Fig. 4 shows two new features: a pronounced jump in contact numbers as one

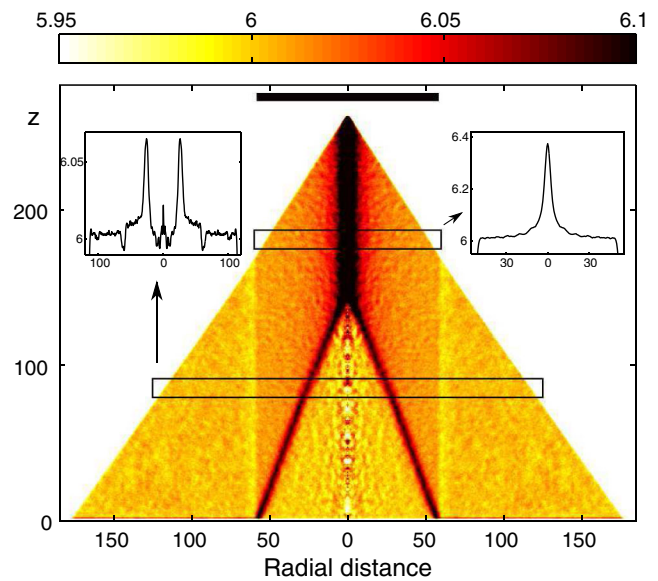


FIG. 4 (color online). The average contact numbers inside of the heap as a function from radial distance from the heap axis. The insets display the variation of contact numbers along the two rectangles, as indicated. Here  $N = 10^7$ .

crosses the boundary from  $A$  to  $C$  and a dip between  $C$  and  $B$ . The boundary between  $A$  and  $C$  corresponds to a “transition zone”, i.e., to the points where the flat surface observed in the earlier stages of the construction of the heap meets the tilted surface. This sharp transition zone corresponds to an area of high contact numbers where the surface curvature is high [see Fig. 1(a)], and therefore, we assume the local surface curvature to be responsible for the changes in the average contact numbers. The local curvature can be determined from the surface  $r(z)$  described above. This assumption is consistent with the peak in contact numbers near the axis (area  $D$ ): close to the top of the heap the mean curvature becomes very high.

As for the dip in contact numbers between areas  $B$  and  $C$ , it corresponds to points where the angle of repose changes from  $\alpha$  to  $\beta$ . Changes in the angle of repose causes lower or even negative mean curvatures, a fact consistent with the drop in the number of contacts. We can explain this as a simple geometrical effect. A particle stopping on a flat surface will have three contacts in addition to the contacts from the particles deposited on top of it. If a particle is deposited onto a surface having a positive mean curvature (e.g., a sphere), it will have three contacts from the particle below it, but thanks to the curved surface, there is more space for contacts from particles deposited on top of it, leading to an increase in the number of contacts. In the case of negative curvature the reverse happens: there is less space for new contacts, causing a decrease in contact numbers.

The angles  $\alpha$ ,  $\beta$ , and  $\gamma$  are not independent from each other, and therefore, we now derive a relation interconnecting them. During the initial phase of the growth, the heap has a flat surface [see the five contours in Fig. 1(a)]. Particles falling onto this flat surface stay on it, since only a quite negligible amount falls off the edge. Particles that fall onto the tilted surface form a layer of approximately constant thickness on the whole inclined surface. From these assumptions and, for simplicity, working with an “average” angle  $\delta = (\alpha + \beta)/2$ , it is not difficult to derive (see Supplemental Material [26]) a differential equation for  $r(h)$ , the function describing how the radius  $r$  of the flat surface shrinks as a function of the height  $h$  of the heap:

$$\frac{dr}{dh} = -\cot\gamma \equiv -\frac{(r + h \cot\delta)^2 - S^2}{(r + h \cot\delta)^2 - r^2} \cot\delta, \quad (1)$$

where  $S$  is the radius of the dropping zone. Of course, this equation is only physically meaningful as long as  $r \geq 0$ . The solution obtained by numerical integration for  $S = 60$  is shown by the straight line in Fig. 1(a). Solving the equation for  $h = 0$ , we get  $\gamma_0 \equiv \gamma(h = 0) = \arctan(2 \tan\delta) = 71^\circ$ . Note that Eq. (1) can be rescaled with respect to  $S$  in such a way that only  $r/S$  and  $h/S$  appear in it. This means that Eq. (1) is scale invariant

and needs to be solved just once, thanks to the relation  $r_S(h) = x r_{S/x}(h/x)$ .

Heaps created using spheres with diameters uniformly distributed in the range  $[0.99, 1.01]$  and  $[0.85, 1.15]$  show a similar duality in the angle of repose, in variations in contact numbers, and in density distribution. Thus, all effects reported here are not effected by small polydispersity.

In conclusion, the analysis of very large 3D heaps of particles proves to be quite revealing. As summarized in Fig. 1(b), we find such heaps to be characterized by several new geometrical features: (i) two external angles of repose  $\alpha$  and  $\beta$ , (ii) an internal angle of repose  $\gamma$ , and (iii) four distinct density (packing fraction) regions,  $A, B, C, D$ . This means that instead of just the familiar single angle of repose [28], heaps may in fact display two distinct angles of repose, a fact implying the existence of four characteristic density zones in the heap. As for the external and internal angles of repose,  $\alpha$  and  $\gamma$ , we showed them to be interrelated according to Eq. (1), a relation that depends of the radius  $S$  of the dropping zone (“rain of particles”). We have also performed an experiment to investigate the impact of noise in the deposition. Such experiments indicated that the duality of the angle of repose may be washed out by moderate to strong noise during the deposition process. We expect the effects described to be easier to observe in rains where grains do not interact (low density rain) and when suppressing the action of inertia, e.g., by performing experiments in an ambient viscous fluid, or building heaps using adhesive particles. Once a particle gets in touch with an already sedimented particle, it still can slowly roll under the action of gravity, but it would not exert any inertial forces. We hope our findings motivate their experimental verification.

This work was supported by the Deutsche Forschungsgemeinschaft through the Cluster of Excellence Engineering of Advanced Materials, Grant No. PO 472/22-1. J.A.C.G. is supported by CNPq, Brazil and by AFOSR, Grant No. FA9550-07-1-0102.

- 
- [1] B. Cambou, M. Jean, and F. Radjai, *Micromechanics of Granular Materials* (Wiley, New York, 2009).
  - [2] *Granular Gas Dynamics*, edited by T. Pöschel and N. Brilliantov (Springer-Verlag, Berlin, 2010).
  - [3] F.H. Hummel and E.J. Finnan, Minutes of Proceedings of the Institution of Civil Engineers **212**, 369 (1921); T. Jotaki and R. Moriyama, *J. Soc. Powder Technol., Jpn.* **16**, 184 (1979); J. Smid and J. Novosad, Powtech Conf. Ind. Chem. Eng. Symp. 63, D3/V/1 (1981).
  - [4] A.P.F. Atman, P. Brunet, J. Geng, G. Reydellet, P. Claudin, R. P. Behringer, and E. Clément, *Eur. Phys. J. E* **17**, 93 (2005).
  - [5] L. Vanel, Ph. Claudin, J.-Ph. Bouchaud, M.E. Cates, E. Clément, and J.P. Wittmer, *Phys. Rev. Lett.* **84**, 1439 (2000).

- [6] S.B. Savage, in *Powder and Grains* 97 (Balkema, Rotterdam, 1997).
- [7] J. Y. Ooi, J. Ai, Z. Zhong, J. F. Cheng, and J. M. Rotter, in *Structures and Granular Solids: From Scientific Principles to Engineering Application*, edited by J. G. Teng *et al.* (Taylor & Francis, London, 2008).
- [8] L. Vanel, D. Howell, D. Clark, R. P. Behringer, and E. Clement, *Phys. Rev. E* **60**, R5040 (1999).
- [9] A. Daerr and S. Douady, *Nature (London)* **399**, 241 (1999).
- [10] A. Higgins, *J. Phys. A* **29**, 2373 (1996).
- [11] M. Shimokawa and S. Ohta, *Phys. Rev. E* **77**, 011305 (2008).
- [12] H. A. Makse, S. Havlin, P. R. King, and H. E. Stanley, *Nature (London)* **386**, 379 (1997).
- [13] R. Jullien and P. Meakin, *Nature (London)* **344**, 425 (1990).
- [14] T. S. Komatsu, S. Inagaki, N. Nakagawa, and S. Nasuno, *Phys. Rev. Lett.* **86**, 1757 (2001).
- [15] E. Altshuler, O. Ramos, E. Martínez, A. J. Batista-Leyva, A. Rivera, and K. E. Bassler, *Phys. Rev. Lett.* **91**, 014501 (2003); E. Martínez, C. Pérez-Penichet, O. Sotolongo-Costa, O. Ramos, K. J. Måløy, S. Douady, and E. Altshuler, *Phys. Rev. E* **75**, 031303 (2007); E. Altshuler, R. Toussaint, E. Martínez, O. Sotolongo-Costa, J. Schmittbuhl, and K. J. Måløy, *Phys. Rev. E* **77**, 031305 (2008).
- [16] T. Shinbrot, *Eur. Phys. J. E* **22**, 209 (2007); T. Shinbrot, N.-H. Duong, M. Hettenbach, and L. Kwan, *Granular Matter* **9**, 295 (2007).
- [17] X.-Z. Kong, M.-B. Hu, Q.-S. Wu, and Y.-H. Wu, *Phys. Lett. A* **348**, 77 (2006).
- [18] C. Urabe, *J. Phys. Soc. Jpn.* **74**, 2475 (2005).
- [19] C. F. M. Magalhães, J. G. Moreira, and A. P. F. Atman, *Eur. Phys. J. E* **35**, 38 (2012); *Phys. Rev. E* **82**, 051303 (2010).
- [20] T. Pöschel, D. Rosenkranz, and J. A. C. Gallas, *Phys. Rev. E* **85**, 031307 (2012); J. A. C. Gallas, H. J. Herrmann, T. Pöschel, and S. Sokołowski, *J. Stat. Phys.* **82**, 443 (1996); T. Pöschel and H. J. Herrmann, *Europhys. Lett.* **29**, 123 (1995); J. A. C. Gallas, H. J. Herrmann, and S. Sokołowski, *Phys. Rev. Lett.* **69**, 1371 (1992).
- [21] P. Roul, A. Schinner, and K. Kassner, *Granular Matter* **13**, 303 (2011); *Geotechnical and Geological Engineering* **29**, 597 (2011).
- [22] Y. Grasselli and H. J. Herrmann, *Eur. Phys. J. B* **10**, 673 (1999).
- [23] W. M. Visscher and M. Bolsterli, *Nature (London)* **239**, 504 (1972).
- [24] R. Jullien and P. Meakin, *Colloids Surf. A* **165**, 405 (2000); R. Jullien, P. Meakin, and A. Pavlovitch, *J. Phys. A* **25**, 4103 (1992).
- [25] I. Goldhirsch and C. Goldberg, *Eur. Phys. J. E* **9**, 245 (2002); *Handbook of Theoretical and Computational Nanotechnology*, edited by M. Rieth and W. Schommers (American Scientific, Valencia, 2006), Vol. 4, pp. 329–386.
- [26] See Supplemental Material at <http://link.aps.org/supplemental/10.1103/PhysRevLett.109.128001> for derivation of Eq. (1). It also presents a simple way of visualizing the pair of angles of repose.
- [27] J. D. Bernal and J. Mason, *Nature (London)* **188**, 910 (1960). See also Refs. [1,2].
- [28] H. Maleki, F. Ebrahimi, and E. N. Oskoe, *J. Stat. Mech.* (2008), P04026.